- Technical Paper -

PLUGGING EFFECT OF WATER ON CARBONATION PROGRESS OF CEMENT PASTE MONITORED BY ^{1}H-NMR RELAXOMETRY MEASUREMENT

Luge CHENG[*1], Ryo KURIHARA[*1], Ippei MARUYAMA [*2, *3]

ABSTRACT

The effect of water content on the carbonation process in cement paste under intermediate (60%) and high (90%) relative humidity (RH) conditions was clarified through water content distribution along the penetration depth. Results reveal that the inhibition of carbonation, due to the water plug effect, occurs at a specific water content level, regardless of whether the RH condition is intermediate (60%) or high (90%). A decreased carbonation degree at the carbonation front over the carbonation duration can be explained by the varying penetration lengths of carbon dioxide.

Keywords: water content, relative humidity, carbonation

1. INTRODUCTION

The carbonation of cementitious materials, owing to the potential to offset carbon dioxide (CO_2) emissions in the concrete industry, has attracted considerable attention. This CO_2 uptake is a multifaceted process, influenced by several factors, including cement type, mix design, and environmental humidity conditions. Notably, the relative humidity (RH) is the one that can be detected during the carbonation process.

Many studies [1][2][3] have investigated the carbonation process in powdered samples or single crystals, such as synthesized C-S-H, ettringite, portlandite, or cement paste powder. These studies controlled RH and CO_2 concentration conditions, overlooking the distribution of water and penetration of CO_2 through the microstructure. The findings indicated that the carbonation rate increases with increasing RH, attributed to a thicker, more continuous water film [3], and enhanced nucleation of calcium carbonate at higher RH conditions [4]. On the other hand, for the carbonation process in hardened cement paste, the diffusion and penetration of water and CO_2 through the microstructure should be considered. Based on the carbonation depth detected by the phenolphthalein solution [5] and the maximum CO_2 adsorption identified through thermogravimetric analysis [6], the optimal RH range for carbonation in hardened cement paste was reported at intermediate humidity range (50-80%). At very high and low RH conditions, the carbonation rate diminished. However, the diffusion of water vapor through the microstructure leads to a heterogeneous water distribution, which does not align with the external RH. Therefore, visualizing the distribution of water content within the cement paste and understanding its impact on the CO_2 diffusion and dissolution during the carbonation is imperative. In this study, the water content in the cement paste during the carbonation process was monitored under accelerated carbonation conditions with intermediate and high RH conditions. Simultaneously, the carbonation depth and phase composition distribution from the surface along the carbonation direction were measured to clarify the effect of water content on the carbonation process.

2. EXPERIMENT METHODS

2.1 Materials and Mix Proportions

Ordinary Portland Cement (OPC) was used in the experiment, with its chemical composition detailed in Table 1 and mineral composition in Table 2. The cement paste was prepared with a water-to-cement ratio (W/C) of 0.55. The deionized water used for mixing was maintained at 20°C for one day prior to use. A planetary

Table 1 Chemical Compositions (%) of the Ordinary Portland cement

CaO	SiO_2	Al_2O_3	Fe_2O_3	MgO	K_2O	Na_2O	SO_3	Cl	SUM
64.19	19.86	5.55	2.80	1.41	0.41	0.28	2.70	0.015	97.22

Table 2 Mineral Composition (%) of Ordinary Portland Cement

C_3S	C_2S	C_3A	C_4AF	Calcite	Bassanite	Gypsum	Periclase	SUM
56.51	18.27	8.55	7.07	4.43	2.78	1.52	0.85	100.0

*1 Dept. of Architecture, the University of Tokyo, JCI Member
*2 Prof., Dept. of Architecture, the University of Tokyo, JCI Member
*3 Prof., Dept. of Environmental Engineering and Architecture, Nagoya University, JCI Member

mixer (ARE-500, THINKY) at 1000 rpm was used for mixing the cement and water. To ensure the homogeneous mixing of the cement paste, initially, a portion of the water was added to the cement to reach a W/C ratio of 0.30 and mixed for 1.5 minutes. Then, more water was incorporated to achieve the target W/C ratio of 0.55, followed by another 1.5 minutes of mixing. After mixing process, the fresh cement paste was placed in 500 mL polypropylene bottles on a roller (IKA ROLLER 10 digital) at 60 rpm for 3.5 hours to minimize the bleeding and segregation. After confirming the cement paste was creamy, it was poured into 5×5×3 cm prismatic molds. The molds were then vibrated to remove entrapped air bubbles. Subsequently, the casting surface was covered with polyethylene wrap, and the molds were stored in a controlled environment at 20℃. The specimens were demolded the next day, sealed, and cured at 20℃ for three months ensuring sufficient hydration of cement before proceeding to the next step of the study.

2.2 Sample Preparation and Exposure

After the curing period, following the JIS standard accelerated carbonation method [7], the samples were sealed on five sides using two-side tapes and covered with water-proof tape, leaving one surface exposed to the controlled environment. This setup was designed to allow CO_2 and moisture penetration from a single direction. The sealed samples were then placed in airtight containers containing saturated salt solutions of NaBr and $BaCl_2$, achieving intermediate and high RH of 58±5% and 91±5%, respectively. To prevent carbonation during the RH controlling process, soda lime particles were added to absorb CO_2. After a 28-day period in each RH-controlled environment, the samples were transferred to carbonation chambers set at a 5% CO_2 concentration and 60% and 90% RH. For each carbonation condition, dummy samples of the same size were also prepared.

2.3 Single Sided NMR

Single-sided Nuclear Magnetic Resonance (NMR) measurements were conducted using the NMR MOUSE PM 25 (Magritek GmbH, Germany) with the Carr-Purcell-Meiboom-Gill (CPMG) technique [8]. Theses measurements were performed both during the RH controlling period at 3, 7, 14, and 28 days, and throughout the carbonation process at 3, 7, 14, 28, 42, and 91 days. The apparatus utilizes a permanent magnet generating a 0.32 T magnetic field B_0 (corresponding to ^{1}H Larmor frequency of 13.12 MHz) with a gradient strength of 300 kHz/mm. A surface Radio Frequency (RF) coil, positioned atop the magnet, is responsible for exciting and detecting the NMR signal from a sensitive spot located 15 mm from the surface of the instrument. The sensitive volume extends approximately 40 × 40 mm^2 in the lateral directions, with a resolution of 200 μm. Since the NMR signal originates from the evaporable water in the cement paste, it allows for correlating the signal intensity with the water content in the sample [9][10]. The specific parameters utilized for CPMG measurements are detailed in Table 3. The echo time and the echo number were selected to cover the entire relaxation process. Sensitive region of measurement was incrementally shifted by 1 mm from the surface to interior part of sample, and the CPMG decays at each depth were fitted to a biexponential decay function to ascertain the associated signal intensities, as shown in Eq. 1:

$$S(t) = A_1 e^{(-t/T_{2,1})} + A_2 e^{(-t/T_{2,2})} \quad (1)$$

where $S(t)$ is the magnetization, t is time, A_1 and A_2 are the magnetization components corresponding to the $T_{2,1}$ and $T_{2,2}$ lifetime constants, associated with water in fine pores (interlayer and gel pore) and coarse pores (interhydrate and capillary pores), respectively.

In addition, a reference water sample was measured using the same parameters, and the resulting CPMG decay was fitted to a single exponential decay function, as expressed in Eq. 2:

$$S_{ref}(t) = A_{ref} e^{(-t/T_2)} \quad (2)$$

Subsequently, the volumetric water content (w) within the sample at each depth was quantified based on the ratio of A_1 and A_2, as illustrated in Eq. 3:

$$w = \frac{A_1 + A_2}{A_{ref}} \quad (3)$$

2.4 Carbonation Depth Measurement

During the carbonation duration, the carbonation depth was determined in the dummy samples at the same intervals as the single-sided NMR measurements under each condition. A segment of the sample was sliced along the carbonation direction and spayed with phenolphthalein solution, followed by taking the images after 24 hours. The conventional method of measuring the carbonation depth—quantifying the distance from the exposed surface to the boundary between the purple (non-carbonated) and colorless (carbonated) areas at five points using vernier calipers [7]—has been noted for its subjectivity and potential for low reproducibility [11]. In this study, we applied a digital image analysis approach using Photoshop software and Python. This method enhances accuracy in determining the carbonation front, involving the following steps [12]: 1) determining the percentage of magenta in both non-carbonated and fully carbonated areas; 2) calculating the midpoint of the magenta percentage between these areas as the indicator

Table 3 Parameters of CPMG measurement

Pulse length (μs)	Number of echoes	Echo time (μs)	Number of scans	Recorded time range (μs)
17	50	75	1024	75-3750

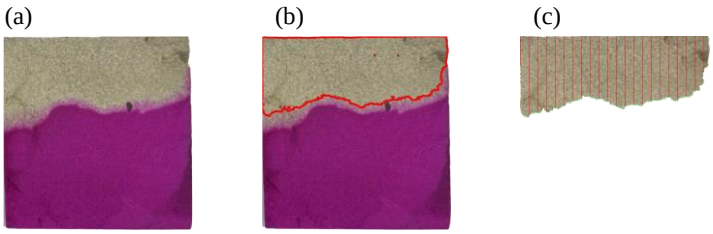

Fig. 1 Procedure of image analysis for carbonation depth: (a) sectional area after spaying phenolphthalein solution; (b) determine the carbonation front according to the magenta percentage of pixel; (c) carbonation depth measured every 1mm from the top side.

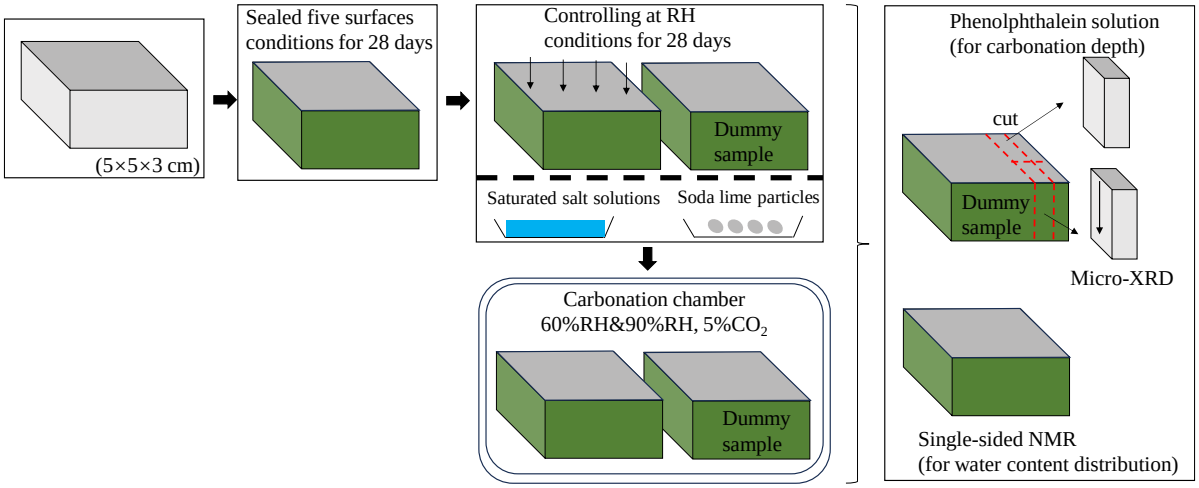

Fig. 2 Overall outline of the experiment

of the carbonation front; 3) identifying pixels in the image corresponding to this midpoint magenta percentage; 4) delineating the entire carbonated area; 5) measuring the distances at 1mm intervals from the top side in the carbonated area; 6) calculating the average value as carbonation depth. Fig. 1 illustrates the image analysis procedure.

2.5 Micro-XRD Mapping

Micro-X-ray diffraction (μ-XRD) mapping measurements were performed using a PANalytical Empyrean diffractometer equipped with Cu Kα radiation.

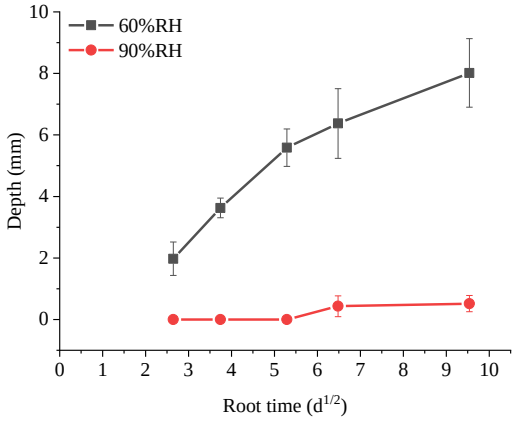

Fig. 3 Carbonation depth under 60%RH and 90%RH conditions

A part of the sample was cut along the carbonation direction from the dummy samples and placed vertically on an X-Y-Z stage in order to measure the XRD patterns of the cement paste at 1 mm interval from the carbonation surface up to 15 mm depth. The scanning range for the 2θ angle was established from 10° to 70°, with a scanning speed of 1.18°/min. Additionally, the maximum irradiated area for single scanning point was about 722 μm.

To provide clarity, the overall experimental outline after curing period is presented in Fig. 2.

3. RESULTS

3.1 Carbonation Depth

Fig. 3 shows that carbonation depth of samples over the carbonation durations, as determined through image analysis after spraying phenolphthalein solution. It is obvious that the carbonation rate increases with the carbonation duration under 60%RH condition and slows down slightly when carbonation duration over 28 days. In contrast, the sectional area of cement paste shows totally magenta color under 90%RH condition until 28 days, and the minor carbonation depths were observed at 42 and 91 days.

3.2 Micro-XRD Mapping Results

The XRD mapping measurements of the

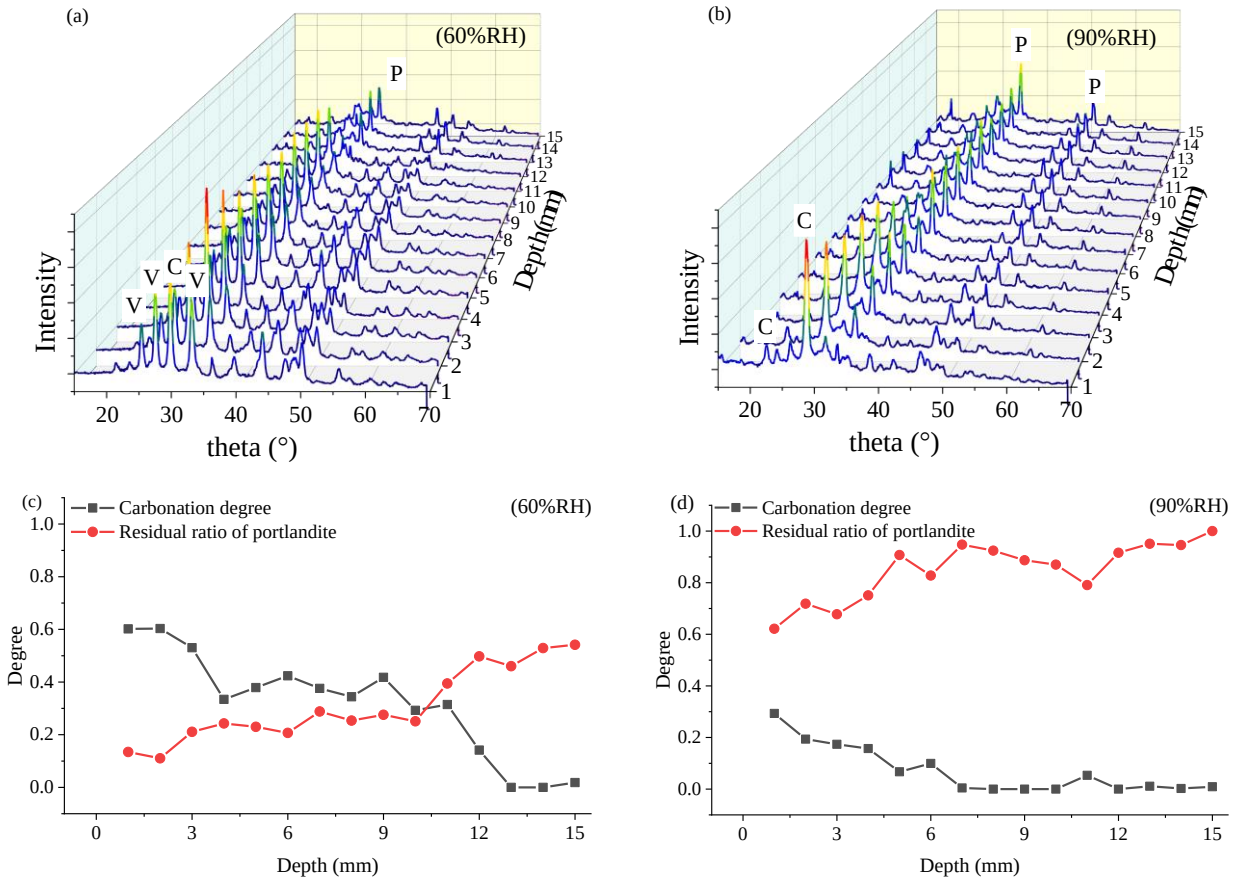

Fig. 4 XRD patterns of sectional area from surface along the carbonation direction under 60%RH (a) and 90%RH (b) conditions at the carbonation duration of 28 days, and the corresponding carbonation degree and residual ratio of portlandite (c), (d).
(P: portlandite; C: calcite, V: vaterite)

carbonated cement paste allowed to track the distribution of carbonation products along the carbonation direction under different RH conditions. Fig.4 (a) and (b) present the example of the XRD patterns at 1 mm interval from the carbonation surface up to 15 mm depth under 60% and 90%RH conditions at 28 days carbonation duration. Under the 60%RH condition, the peaks of calcium carbonate are prominent across the carbonation depth, while peaks of portlandite show a slight increase as the depth increases. Under 90%RH condition, the distinct peaks of calcium carbonate are observed at the surface area to a depth of 5 mm, beyond which there is a marked decrease, while the intensity of portlandite peaks increases with increasing depth. The corresponding areas of the diffraction peak of each phase were calculated with the baseline determined by the lowest values at both end-part of corresponding peak. The ratios of the peak area of calcium carbonate and portlandite to the sum of peak areas in non-carbonated area were treated as the initial value of calcium carbonate (C_{ini} = 4%) and the initial value of portlandite (P_{ini}= 96%); and the ratios of peak area of calcium carbonate and portlandite to the sum of peak areas at the carbonated surface under 60%RH were considered as the maximum value of calcium carbonate (C_{max}= 97%), and minimum value of portlandite (P_{min}= 3%). The carbonation degree (D_C) at each position was then calculated based on the area of calcium carbonate peaks (C) as follows:

$$D_C = \frac{C - C_{ini}}{C_{max} - C_{ini}} \quad (3)$$

The residual ratio of portlandite (R_P) was then calculated based on the area of portlandite peaks (P) as follows:

$$R_P = \frac{P_{ini} - P}{P_{ini} - P_{min}} \quad (4)$$

The results of carbonation degrees and residual ratios of portlandite at each depth under 60%RH and 90%RH conditions for 28 days were shown in Fig. 4 (c) and (d) as an example.

3.3 Water Content Distribution

Fig. 5 shows the distribution of water content along the penetration direction from the exposed surface during both the RH controlling process (denoted by empty marks) and the carbonation process (denoted by solid marks). During the RH controlling process until 28 days under 60%RH, a continuous decrease in water content with increasing penetration depth was observed,

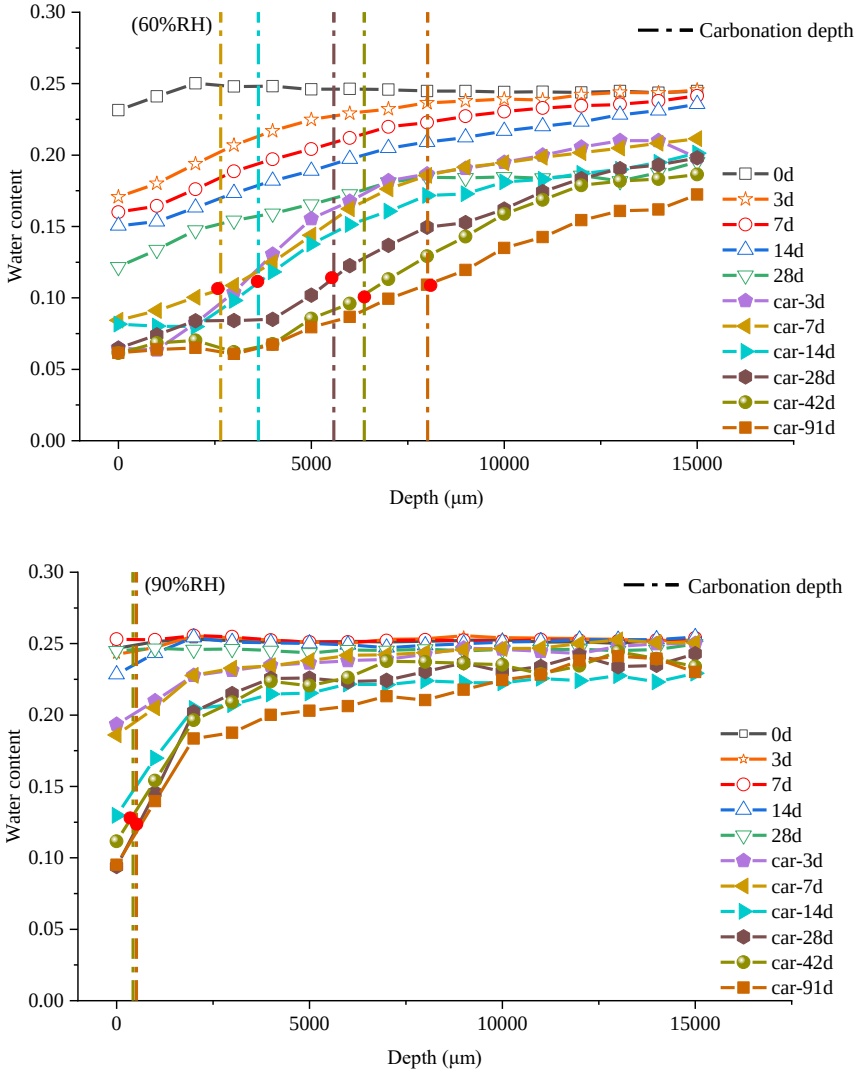

Fig. 5 Volumetric water content distribution during RH controlling and accelerated carbonation process (red points represent the interception of water content and carbonation depth)

more pronounced near the surface due to greater evaporation. In contrast, the water content remained constant under the 90%RH condition. Following carbonation, a significant decrease in water content was observed in the carbonated areas under both conditions. The carbonation fronts, represented by dashed lines at each carbonation duration, consistently stagnated at similar water contents: between 0.10 and 0.12 under 60%RH, and around 0.12 under 90%RH, as indicated by the red points in the figure.

4. DISCUSSION

As commonly agreed in previous research, the intermediate RH is optimal for carbonation due to the existence of sufficient water for the carbonation reaction alongside adequate space for CO_2 diffusion. At higher RH condition, water saturation in pores plugs the penetration of CO_2, thus hindering diffusion [5][6]. This phenomenon can be confirmed from the faster carbonation rate under 60%RH compared to 90%RH condition. However, due to the heterogeneous microstructure of cementitious materials, the water content within the sample does not always equilibrate with the ambient RH [13]making RH a less imprecise indicator for the water plug effect on the carbonation process. Even under the intermediate RH conditions, the internal water content tends to be higher than near the surface due to lower evaporation rates, leading to a stepwise distribution of water content, making the CO_2 penetrate through the outer regions. Beyond a certain depth, however, increased water saturation restricts CO_2 diffusion, causing the carbonation front to stagnate at a specific water content. This is demonstrated in Fig. 5, where the carbonation front consistently stalls at a water content range of 0.10 to 0.12, regardless of the RH level. The notably slow carbonation depth observed under 90% RH can be attributed to a slower water movement from inside to outside, maintaining a higher water content near the surface and thus inhibiting carbonation.

Furthermore, Table 4 presents the carbonation degree at the carbonation front, calculated using Eq. 1 for carbonation durations of 7, 14, 28, 42 and 91 days under 60%RH and 90%RH conditions.

Under 60%RH condition, a decrease trend in the carbonation degree at the carbonation front is observed over the carbonation duration. This trend can be attributed to diminishing dissolved CO_2 concentration as the penetration length increases, consequently, a reduced carbonation degree at different carbonation fronts. On the other hand, the carbonation degree of the carbonation front under 90%RH is slightly lower even at the similar water content levels due to the distance from carbonation front to the surface is smaller than the 1 mm step used for XRD mapping. Hence, the measured range at the surface includes part of the non-carbonated area.

Table 4 Carbonation degrees (%) at carbonation front under 60% RH and 90% RH conditions

Carbonation duration (d)	7	14	28	42	91
60%RH	63.3	49.2	43.4	37.5	37.6
90%RH	-	-	-	36.3	42.2

During the carbonation process, the water content within the carbonated area remains constant at 42 and 91 days up to a depth of 4 mm under 60%RH, while within the surface area under 90%RH condition. This consistency of water content can be attributed to the densified and stable microstructure near the surface due to adequate carbonation (the average carbonation degrees at carbonated area up to 4 mm under 60%RH are 97.8%, 98.9% at 42 and 91 days; the average carbonation degree at 1mm depth are 95.2% and 100.0% at 42 and 91 days). The corresponding higher water content value near the surface under 90%RH, compared to 60%RH, aligns with the Kelvin-Laplace theory[14], indicating increased water condensation at higher RH levels.

5. CONCLUSIONS

This study quantitatively analyzed and visualized the water content distribution during the accelerated carbonation process with 5% CO_2 concentration at 20°C under both intermediate (60%) and high (90%) RH conditions. Key findings include:

1) The inhabitation effect on carbonation by water plug was observed to occur at a specific water content level, irrespective of the RH conditions being intermediate or high.
2) The carbonation rate is lower under high RH condition than intermediate RH condition, attributed to slower water movement from interior towards the surface, resulting in a higher water content near the surface and consequently, inhibiting the carbonation.
3) The decreasing carbonation degrees at the carbonation front with the carbonation durations, despite similar water content levels, can be attributed to the varying penetration length of CO_2.

ACKNOWLEDGEMENT

This study was based on the results obtained from a project (JPNP21023) commissioned by the New Energy and Industrial Technology Development Organization (NEDO).

REFERENCES

[1] S. Steiner, B. Lothenbach, T. Proske, A. Borgschulte, and F. Winnefeld, “Effect of relative humidity on the carbonation rate of portlandite, calcium silicate hydrates and ettringite,” *Cem. Concr. Res.*, vol. 135, no. May, 2020.

[2] R. M. Dheilly, J. Tudo, Y. Sebaibi, and M. Quéneudec, “Influence of storage conditions on the carbonation of powdered Ca(OH)2,” *Constr. Build. Mater.*, vol. 16, no. 3, pp. 155–161, 2002.

[3] S. M. Shih, C. S. Ho, Y. S. Song, and J. P. Lin, “Kinetics of the reaction of Ca(OH)2 with CO_2 at low temperature,” *Ind. Eng. Chem. Res.*, vol. 38, no. 4, pp. 1316–1322, 1999.

[4] I. Galan, F. P. Glasser, D. Baza, and C. Andrade, “Assessment of the protective effect of carbonation on portlandite crystals,” *Cem. Concr. Res.*, vol. 74, pp. 68–77, 2015.

[5] E. Drouet, S. Poyet, P. Le Bescop, J. M. Torrenti, and X. Bourbon, “Carbonation of hardened cement pastes: Influence of temperature,” *Cem. Concr. Res.*, vol. 115, no. September 2018, pp. 445–459, 2019.

[6] I. Galan, C. Andrade, and M. Castellote, “Natural and accelerated CO_2 binding kinetics in cement paste at different relative humidities,” *Cem. Concr. Res.*, vol. 49, pp. 21–28, 2013.

[7] Japanese Industrial Standard Committee: Tokyo, *JIS A 1153; 2012, Method of Accelerated Carbonation Test for Concrete*. 2012.

[8] S. Meiboom and D. Gill, “Modified Spin-Echo Method for Measuring Nuclear Relaxation Times,” *Rev. Sci. Instrum.*, vol. 29, no. 8, pp. 688–691, Aug. 1958.

[9] M. Van Landeghem, J. B. D’Espinose De Lacaillerie, B. Blümich, J. P. Korb, and B. Bresson, “The roles of hydration and evaporation during the drying of a cement paste by localized NMR,” *Cem. Concr. Res.*, vol. 48, pp. 86–96, 2013.

[10] T. Colinart and P. Glouannec, “Investigation of drying of building materials by single-sided NMR,” *Energy Procedia*, vol. 78, pp. 1484–1489, 2015.

[11] J. Il Choi, Y. Lee, Y. Y. Kim, and B. Y. Lee, “Image-processing technique to detect carbonation regions of concrete sprayed with a phenolphthalein solution,” *Constr. Build. Mater.*, vol. 154, pp. 451–461, 2017.

[12] R. G. da Silveira and G. C. Isaia, “Proposal of a digital image analysis method for determining the carbonated front in concretes,” *Ambient. Construído*, vol. 22, no. 3, pp. 275–298, 2022.

[13] W. Kubissa, “Permeability testing of radiation shielding concrete manufactured at industrial scale,” vol. 0, 2018.

[14] P. Lura, O. M. Jensen, and K. van Breugel, “Autogenous shrinkage in high-performance cement paste: An evaluation of basic mechanisms,” *Cem. Concr. Res.*, vol. 33, no. 2, pp. 223–232, Feb. 2003.